



OPEN

A combination model of CT-based radiomics and clinical biomarkers for staging liver fibrosis in the patients with chronic liver disease

Maowen Tang^{1,4}, Yuhui Wu^{1,4}, Na Hu^{1,4}, Chong Lin¹, Jian He¹, Xing Xia¹, Meihua Yang², Pinggui Lei^{1,2}✉ & Peng Luo^{2,3}✉

A combined model was developed using contrast-enhanced CT-based radiomics features and clinical characteristics to predict liver fibrosis stages in patients with chronic liver disease (CLD). We retrospectively analyzed multiphase CT scans and biopsy-confirmed liver fibrosis. 160 CLD patients were randomly divided into 7:3 training/validation ratio. Clinical laboratory indicators associated with liver fibrosis were identified using Spearman's correlation and multivariate logistic regression correlation. Radiomic features were extracted after segmenting the entire liver from multiphase CT images. Feature dimensionality reduction was performed using RF-RFE, LASSO, and mRMR methods. Six radiomics-based models were developed in the training cohort of 112 patients. Internal validation was conducted on 48 randomly assigned patients. Receptor Operating Characteristic (ROC) curves and confusion matrices were constructed to evaluate model performance. The radiomics model exhibited robust performance, with AUC values of 0.810 to 1.000 for significant fibrosis, advanced fibrosis, and cirrhosis. The integrated clinical-radiomics model had superior diagnostic efficacy in the validation cohort, with AUC values of 0.836 to 0.997. Moreover, these models outperformed established biomarkers such as the aspartate aminotransferase to platelet ratio index (APRI) and the fibrosis 4 score (FIB-4), as well as the gamma glutamyl transpeptidase to platelet ratio (GPR), in predicting the fibrotic stages. The clinical-radiomics model holds considerable promise as a non-invasive diagnostic tool for the assessment and staging of liver fibrosis in the patients with CLD, potentially leading to better patient management and outcomes.

Keywords Radiomics, Contrast-enhanced CT, Liver fibrosis, Prediction model, Chronic liver disease

Abbreviations

A/G	Albumin-globulin ratio
ALB	Albumin
ALP	Alkaline phosphatase
ALT	Alanine aminotransferase
APRI	Aspartate aminotransferase to platelet ratio index
AST	Aspartate aminotransferase
AUC	Area under the curve
HBV	Hepatitis B virus
CKMB	Creatine kinase-MB
CLD	Chronic liver disease
CRP	C-reactive protein

¹Department of Radiology, Affiliated Hospital of Guizhou Medical University, Guiyang of Guizhou 550004, China. ²School of Public Health, Guizhou Medical University, Guiyang of Guizhou 550004, China. ³The Key Laboratory of Environmental Pollution Monitoring and Disease Control, Ministry of Education, Guizhou Medical University, Guiyang of Guizhou, China. ⁴These authors contributed equally: Maowen Tang, Yuhui Wu and Na Hu. ✉email: pingguilei@foxmail.com; luopeng@gmc.edu.cn

CT	Compute tomography
cTn	Cardiac troponin
DBiL	Direct bilirubin
DCA	Decision curve analysis
FIB-4	Fibrosis 4 score
FOV	Field of view
GGT	Gamma-glutamyl transferase
GLB	Globulin
GPR	Gamma glutamyl transpeptidase to platelet ratio
HB	Hemoglobin
HDL-C	High-density lipoprotein cholesterol
ICC	Intra-class correlation coefficient
IRB	Institutional review board
LASSO	Least absolute shrinkage and selection operator
LDL-C	Low-density lipoprotein cholesterol
LP	Lipoprotein
MRI	Magnetic resonance imaging
mRMR	Minimum redundancy maximum relevance
MSCT	Multi-slice computed tomography
MYO	Myoglobin
PBNP	Pro-B-type natriuretic peptide
PLT	Platelet
Radscore	Radiomics quality score
RBC	Red blood cell
RF-RFE	Random forest recursive feature elimination
ROC	Receiver operating characteristic curve
TBA	Total bile acid
TBIL	Total bilirubin
TC	Total cholesterol
TP	Total protein
UR	Urea
US	Ultrasonography
VIF	Variance inflation factor
WBC	White blood cell

Global public health is significantly impacted by chronic liver disease (CLD). Liver fibrosis may progress to cirrhosis, complications related to portal hypertension, and even hepatocellular cancer, which is closely linked to high morbidity and mortality in CLD¹. Therefore, it is crucial to diagnose liver cirrhosis and quantify liver fibrosis as early as possible in the management of chronic liver disease². The gold standard for staging liver fibrosis is liver biopsy. However, it carries the risk of procedure-related complications, such as severe bleeding, organ damage, pain, and death, and has limitations related to sampling error, inter-observer variability, semi-quantitative results, and high cost³.

In clinical practice, the extent of liver fibrosis is commonly evaluated using serum biomarkers. Serum markers, including aspartate aminotransferase to platelet ratio index (APRI) and the fibrosis 4 score (FIB-4), as well as the gamma glutamyl transpeptidase to platelet ratio (GPR) rely on clinical and biochemical indicators including serum aspartate aminotransferase (AST), alanine aminotransferase (ALT) levels, and serve as viable alternatives to liver biopsy for monitoring changes in liver fibrosis caused by various factors⁴. However, there are also limitations to these metrics, since the biomarkers do not target a particular organ and their measurement is highly dependent on how quickly they are excreted and cleared⁵. A number of imaging-based methods have been investigated to evaluate the extent of liver fibrosis^{6–9}. Magnetic resonance imaging (MRI) and ultrasonography (US) elastography have been the most successful methods for measuring liver stiffness in clinical practice^{7,8}. Nevertheless, inaccuracies in measuring deep liver tissues, and their usability and clinical relevance are compromised by the fact that ascites or severe obesity can significantly affect their performance. The 2018 American Association for the Study of Liver Diseases (AASLD) Practice Guidelines suggest using multi-phase CT or MRI for initial diagnosis in high-risk patients with abnormal monitoring results¹⁰. Enhanced CT offers more information than plain CT scans and has advantages over MRI, including lower cost, fewer contraindications, widespread availability, and excellent whole-organ imaging capabilities¹¹. However, CT enhancement has drawbacks like radiation exposure and potential iodine allergies.

Radiomics can turn images into extensive quantitative data, enabling the extraction of additional biological information¹². As a clinical decision-making tool in liver diseases, radiomics analysis primarily aims to detect hepatocellular carcinoma¹³, diagnose indeterminate hepatic nodules¹⁴, and assess the risk of recurrence of hepatocellular carcinoma¹⁵. The utilization of radiomics for identification of distinct presentations of liver disease, like clinically significant portal hypertension¹⁶ and hepatic fibrosis staging^{17–19}, has not been extensively investigated in previous studies. It remains uncertain which phase, arterial, venous, or delayed, has the potential to improve the accuracy of liver fibrosis staging analysis.

The objective of this study was to investigate whether adding routine clinical biomarkers to radiomics signatures improves the accuracy of liver fibrosis staging using CT-based radiomics data. The secondary aim was to

compare the accuracy of the clinical-radiomic model and specific clinical indicators in diagnosing liver fibrosis severity.

Materials and methods

The Institutional Review Board (IRB) at the Affiliated Hospital of Guizhou Medical University approved this retrospective study. The study adhered to ethical guidelines. Patient confidentiality and data protection measures were strictly followed to ensure privacy and anonymity.

Patients

The dataset comprises multi-phase abdominal CT enhanced imaging and liver histopathological examination data from 110 patients who were treated at our hospital between 2017 and 2022.

Inclusion criteria were: (1) Patients with chronic liver disease. (2) Multiphase contrast agent-enhanced CT examinations. (3) Pathologic findings within 1 month of CT examination. (4) No previous liver surgery or evidence of malignant tumors. Exclusion criteria were: (1) Lack of enhanced CT images. (2) Incomplete clinical data, such as incomplete laboratory data or histologic staging. (3) Poor image quality preventing analysis, such as heavy image artifacts. (4) The focal liver lesions detected by CT images (maximum diameter > 5 cm). (5) History of previous liver surgery. Following these criteria, 826 cases of chronic liver disease were initially collected, with 716 patients excluded, leaving a final inclusion of 110 eligible patients (Fig. 1).

Additionally, the dataset includes CT-enhanced imaging data from 50 patients diagnosed with cirrhosis. The enhanced images of these 50 cases of decompensated cirrhosis, which are characterized by wavy margins of the liver, portal hypertension, splenomegaly, and ascites, were selected by two radiologists with 8 years of clinical experience in abdominal radiology (Fig. 1).

Pathological stages of liver fibrosis

110 patients with CLD had confirmed histological results by pathological biopsy. The liver samples were examined by an experienced pathologists who was blinded to the clinical and laboratory data, using the Scheuer scoring system²⁰. The stages of liver fibrosis were as follows: S0(no fibrosis), S1(mild fibrosis, no septum), S2 (moderate fibrosis, few intervals), S3(severe fibrosis, many intervals, no cirrhosis), S4 (cirrhosis). According to this study, pathological stage \geq S2 and \geq S3 were used to define significant fibrosis and advanced fibrosis, respectively.

50 patients of enhanced images from cirrhotic patients were selected by two radiologists and classified as stage S4 (cirrhosis).

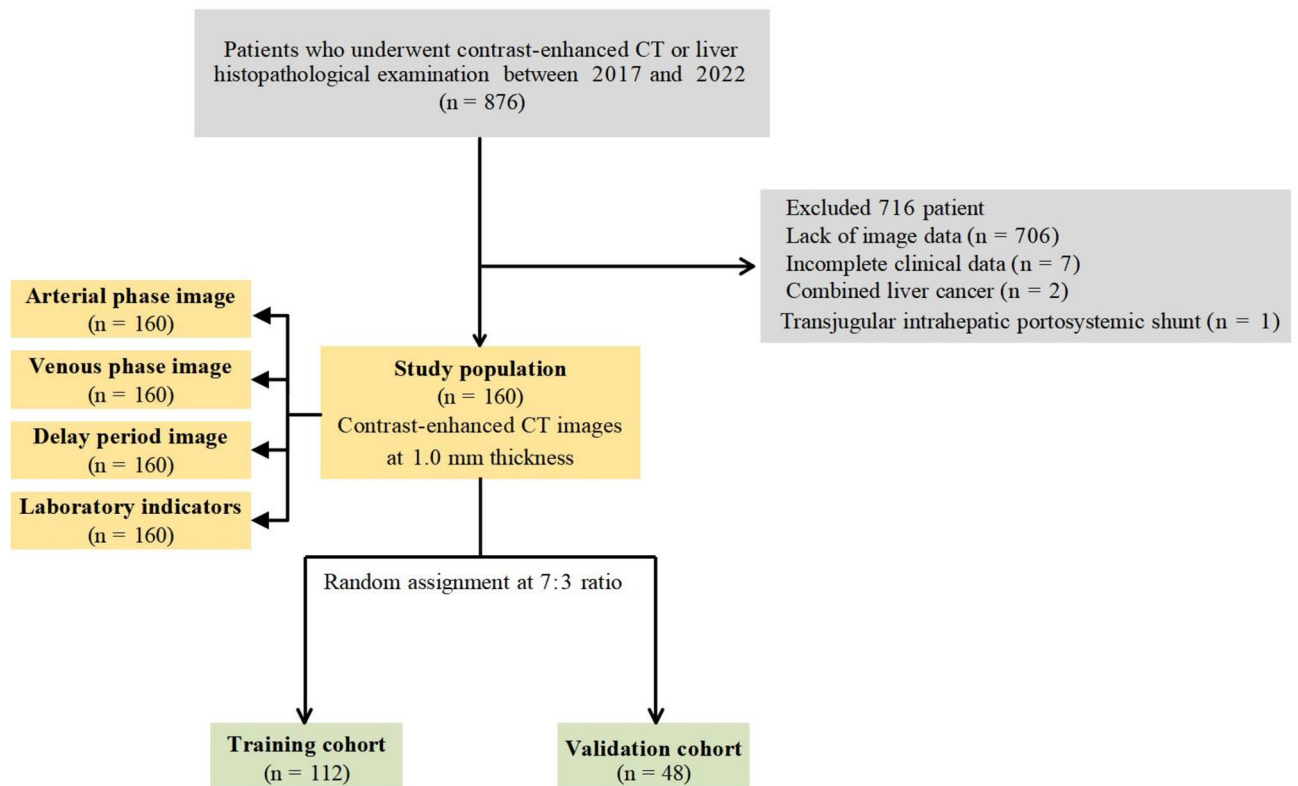


Fig.1. The flowchart of this study.

CT image acquisition

The patient's abdominal enhanced digital medical images were retrieved from the Picture Archiving and Communication System (PACS) of the Affiliated Hospital of Guizhou Medical University.

The patients primarily underwent imaging using 128-slice MSCT scanner (SOMATOM Definition AS+, Siemens, Germany). The scanning range covered the upper abdomen.

Radiomic feature extraction and selection

Enhanced 1 mm DICOM images of 160 patients were converted to neuroimaging informatics technology initiative (NIfTI) image and automatically segmented using 3D-Unet liver segmentation model. Manual modification after the liver segmentation was performed using 3D Slicer (V5.3.0, <https://www.slicer.org/>). Pyradiomics was used to extract radiomic texture features from enhanced images of 160 patients. Feature stability was assessed by randomly selecting 40 patients and performing segmentation twice, with intra-class correlation coefficient (ICC) used to retain only features with values greater than 0.8 for subsequent analysis. Z-scores normalized stable radiomic features values. Next, We employed the Spearman correlation coefficient ($p < 0.05$) to assess the correlation between stable radiomic features and fibrosis staging. To address the high number of features, we used random forest recursive feature elimination (RF-RFE) to select the top 50 features, and least absolute shrinkage and selection operator (LASSO) to reduce the feature. If the features still exceed 10 features, we employed the minimum redundancy maximum relevance (mRMR) method to select the most representative features count to 10 or below for support vector classifier (SVC) modeling. The parameters of the SVC model were determined through grid search, which was manually tuned to achieve the best performance and obtain the most optimal results. The training set underwent 10 repetitions of random 5-fold cross-validation, this process involves training data and testing data. The penalty parameter was fine-tuned during this process. The same method is used to process images in the arterial phase, venous phase, and delayed phase. The final model evaluation involved the use of area under the curve (AUC) and confusion matrix.

The radiomics quality score (Radscore) is calculated from the linear combination of features selected by LASSO and the weighting coefficients corresponding to each radiomic feature. The calculation formula for Radscore is as follows:

$$\text{Radscore} = \beta_1 * X_1 + \beta_2 * X_2 + \beta_3 * X_3 + \dots + \beta_i * X_i, \quad (1)$$

where β_1 - β_i represent the coefficients of the variables selected through LASSO analysis, and X_1 - X_i represent the corresponding values of these variables. (Fig. 2) shows a concise flow diagram that clarifies the entire study.

Clinical factors selection

In the selection of clinical factors, we implemented a three-step process. First, preliminary screening of factors with significant correlations was carried out using Spearman correlation analysis ($P < 0.05$). Second, multivariate logistic regressions with backward stepwise selection was applied to choose the factors for predicting significant fibrosis stage. Third, the variance inflation factor (VIF) is used to exclude collinearity among variables, where VIF greater than 10 will be excluded²¹. The APRI, FIB-4, and GRP were determined through the application of the following formulas.²²²²²²²²²²

$$\text{APRI} = \frac{(\text{AST}(\text{IU/L})/\text{ULN}) \times 100}{\text{PLT} (10^9/\text{L})} \quad (2)$$

$$\text{FIB} - 4 = \frac{\text{AGE}(\text{years}) \times \text{AST}(\text{IU/L})}{\text{PLT}(10^9/\text{L}) \times \text{ALT}(\text{IU/L})^{1/2}} \quad (3)$$

$$\text{GPR} = \frac{(\text{GGT}(\text{IU/L})/\text{ULN}) \times 100}{\text{PLT}(10^9/\text{L})} \quad (4)$$

In the formula (2),(3),(4), ULN represents the upper limit of the normal value, and PLT refers to the platelet count, expressed in terms of platelets per liter (10^9). An integrated SVC model was created by combining the radiomics signature with clinical biomarkers.

Statistical analysis

Mean \pm SD represented continuous variables analyzed through Kruskal–Wallis rank test. Categorical variables were represented as proportions and analyzed by Chi-squared or Fisher's exact test. Reliability was assessed using the ICC, with consistency divided into poor (< 0.5), medium (0.51–0.80), good (0.81–0.89) or excellent (≥ 0.9). The nomogram model was constructed based on the Radscore and clinical risk factors. The AUC was employed to assess the predictive accuracy of the models. The threshold value is determined by the F1-score index, which is an ideal combination of sensitivity and specificity. The corresponding sensitivity, specificity and accuracy were estimated. The prediction performance was further assessed by decision curve analysis (DCA) to determine its clinical utility. A two-sided $p < 0.05$ was considered statistically significant. All statistical analyses were conducted in R software (version 4.3.0, <https://cran.r-project.org/src/base/R-4/>) and Python (version 3.8.2, <https://www.python.org/downloads/release/python-382/>).

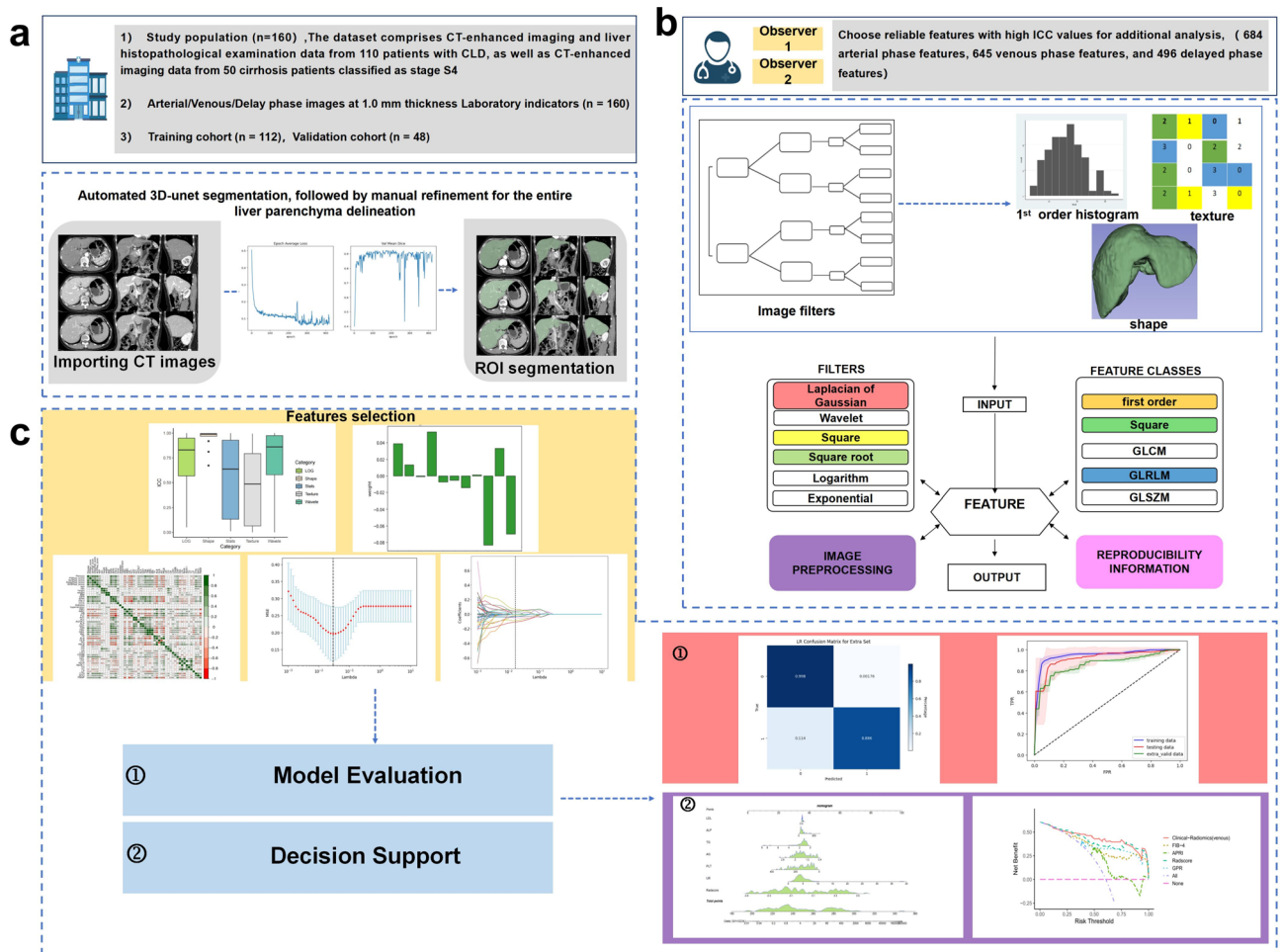


Fig.2. The radiomic workflow. The procedure encompassing tasks such as ROI segmentation, features extraction, features selection, clinical application and analysis. (a) Achieving automatic segmentation of the entire liver ROI on enhanced CT images using 3D-UNET. followed by manual refinement for the entire liver parenchyma delineation. (b) Extracted radiomic features, including first-order statistics, textural features, and wavelet-based. transformations. (c) Models were developed using SVC, including the Radscore_{arterial/venous/delayed} model and the Clinical-Radiomics_{arterial/venous/delayed} model. The performance of the established models was evaluated using ROC curves, DCA curves, and confusion matrices. ROC, receiver operator characteristic, DCA, decision curve analysis.

Results

Study population

We acquired comprehensive demographic and clinical information about the patients (Table 1). Pathological staging of liver fibrosis (S0-S4) corresponds to arterial, venous, and contrast-enhanced CT images as presented in (Fig. 3).

Identification of predictive clinical factors

Routine clinical factors including Creatine Kinase-MB (CKMB), Hemoglobin (HB), AST, Alkaline phosphatase (ALP), Gamma-glutamyl transferase (GGT), Total bile acid (TBA), Total bilirubin (TBIL), Direct bilirubin (DBiL), Urea (UR), Red blood Cell (RBC), C-reactive protein (CRP), Albumin-globulin ratio (A/G), High-density lipoprotein cholesterol (HDL-C), Low-density lipoprotein cholesterol (LDL-C), Total Cholesterol (TC), Lipoprotein (LP), Myoglobin (MYO) and Pro-B-type natriuretic peptide (PBNP) were also related to significant fibrosis ($P < 0.05$ for all). A multivariable logistic regression analysis identified PLT, ALP, A/G, UR, LDL-C, and TC as independent predictors for significant fibrosis (Table 2). We have developed a clinical model based on the comprehensive analysis of PLT, ALP, A/G, UR, LDL-C, and TC laboratory indicators. The AUC results of the clinical model are 0.811, 0.850, and 0.953 for significant fibrosis, advanced fibrosis, and cirrhosis (Table 3).

Identification of predictive FIB-4 APRI GPR

The analysis encompassed the selection of specific clinical biomarkers, namely APRI, FIB-4, and GPR. The AUC of the APRI model is 0.757 in the diagnosis of significant fibrosis, while the AUCs were 0.796 and 0.821 in the

Variables	Total number	Histologic stages					P value
		S0	S1	S2	S3	S4	
Patient	160	29	37	26	12	56	
Age(years)		43.1 ± 10.1	42.8 ± 12.4	43.9 ± 11.3	47.2 ± 9.1	53.0 ± 11.7	<0.001
Sex							0.398
Male	92	15 (51.7%)	19 (51.4%)	16 (61.5%)	5 (41.7%)	37 (66.1%)	
Female	68	14 (48.3%)	18 (48.6%)	10 (38.5%)	7 (58.3%)	19 (33.9%)	
AST(U/L)		40.3 ± 38.4	71.1 ± 92.1	84.9 ± 91.0	81.3 ± 85.9	94.5 ± 100.9	<0.001
ALT(U/L)		60.4 ± 86.2	111.2 ± 168.2	117.6 ± 188.5	79.6 ± 96.0	71.4 ± 101.6	0.273
PLT(10 ⁹ /L)		191.9 ± 72.2	190.4 ± 72.2	166.2 ± 55.6	145.2 ± 60.0	81.7 ± 57.1	<0.001
TBA(μmol/L)		5.6 ± 11.2	10.8 ± 15.2	28.3 ± 48.4	28.6 ± 38.1	74.3 ± 77.1	<0.001
GPR		0.9 ± 1.2	0.9 ± 1.0	2.5 ± 3.4	2.9 ± 3.1	6.4 ± 10.6	<0.001
APRI		0.7 ± 0.7	1.4 ± 1.9	1.9 ± 3.1	1.8 ± 2.5	4.4 ± 4.7	<0.001
FIB-4		1.5 ± 1.0	1.9 ± 1.5	2.7 ± 2.6	3.1 ± 2.0	10.6 ± 9.1	<0.001
Etiology of liver fibrosis							
HBV	83	17 (20.5%)	15 (18.1%)	11 (13.3%)	6 (7.2%)	34 (41.0%)	
HCV	6	0 (0.0%)	3 (50.0%)	0 (0.0%)	0 (0.0%)	3 (50.0%)	
NAFLD	2	0 (0.0%)	1 (50.0%)	1 (50.0%)	0 (0.0%)	0 (0.0%)	
PBC	6	0 (0.0%)	0 (0.0%)	1 (16.7%)	2 (33.3%)	3 (50.0%)	
AIH	8	0 (0.0%)	0 (0.0%)	3 (37.5%)	2 (25.0%)	3 (37.5%)	
ALC	13	1 (7.7%)	1 (7.7%)	2 (15.4%)	0 (0.0%)	9 (69.2%)	
DIH	6	1 (16.7%)	1 (16.7%)	3 (50.0%)	1 (16.7%)	0 (0.0%)	
Other	36	10 (27.8%)	16 (44.4%)	5 (13.9%)	1 (2.8%)	4 (11.1%)	

Table 1. Patient characteristics. Except where indicated, data are numbers of patients, with percentages in parentheses. *ALT* alanine aminotransferase, *AST* aspartate aminotransferase, *PLT* platelet, *TBA* total bile acid, *GPR* gamma glutamyl transpeptidase to platelet ratio, *APRI* aspartate transaminase to platelet ratio, *FIB-4* Fibrosis 4 score, *HBV* hepatitis B virus, *HCV* hepatitis C virus, *NAFLD* non-alcoholic fatty liver disease, *PBC* primary biliary cirrhosis, *AIH* autoimmune hepatitis, *ALC* alcoholic liver cirrhosis, *DIH* drug-induced hepatitis.

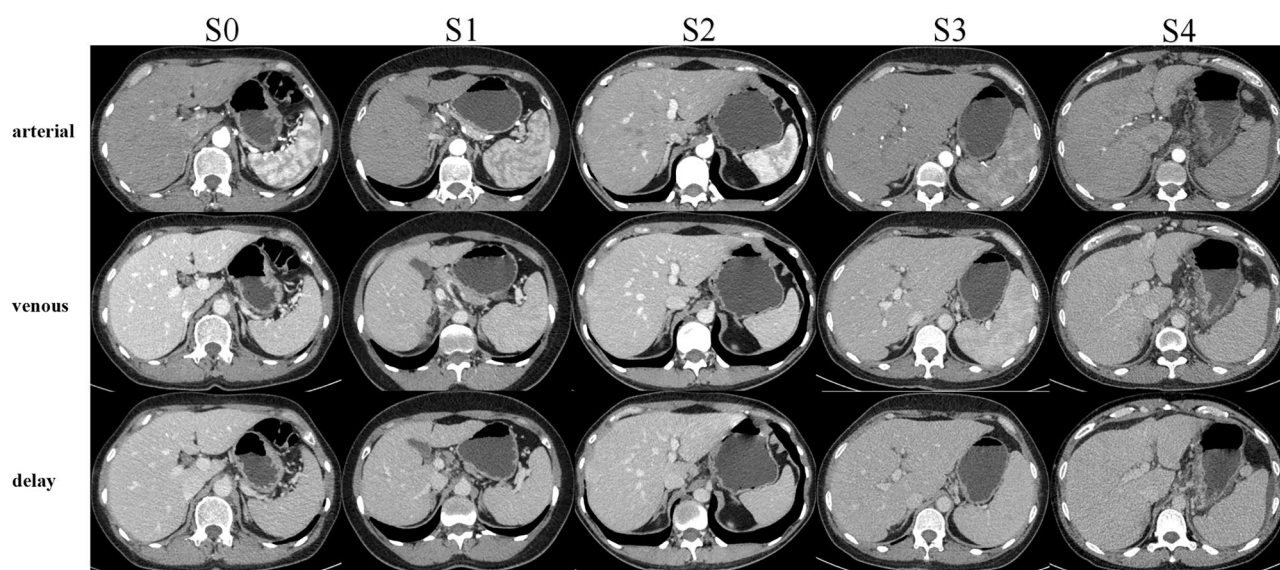


Fig. 3. The changes in the arterial, venous, and delayed phases of enhanced CT images from S0 to S4. In S01, the liver appears normal on imaging. In S2-4, the portal vein widens and the liver-spleen volume ratio decreases. By S4, the liver edge exhibits a wavy pattern of changes, and the liver fissures become wider. Multiple tortuous small blood vessels are observed in the gastric fundus, along with ascites.

Variable	Spearman correlation analysis		Multivariable analysis		Collinearity statistics
	Coefficient	P value	b coefficient (95%CI)	P value	VIF
PLT(10 ⁹ /L)	-0.625	< 0.001	0.978 (0.969–0.987)	< 0.001	1.4
ALP (U/L)	0.279	< 0.001	1.015 (1.006–1.025)	0.001	1.3
A/G	-0.499	< 0.001	0.050 (0.012–0.219)	< 0.001	1.1
UR(mg/dL)	0.202	0.010	1.475 (1.050–2.071)	0.025	1
LDL-C(mmol/L)	-0.316	< 0.001	14.088 (1.897–104.621)	0.009	9.4
TC(mmol/L)	-0.303	0.001	0.112 (0.023–0.545)	0.007	9.7
Age (years)	0.354	< 0.001	0.999 (0.958, 1.041)	0.950	NA
RBC(10 ⁹ /L)	-0.461	< 0.001	1.440 (0.533, 3.895)	0.472	NA
WBC (10 ⁹ /L)	-0.259	< 0.001	0.906 (0.777, 1.055)	0.204	NA
HB(g/L)	-0.427	< 0.001	1.006 (0.982, 1.032)	0.611	NA
AST(U/L)	0.351	< 0.001	0.998 (0.995, 1.001)	0.163	NA
AST/ALT	0.333	< 0.001	1.503 (0.644, 3.508)	0.346	NA
GGT(U/L)	0.358	< 0.001	1.001 (0.999, 1.002)	0.523	NA
TBA(umol/L)	0.618	< 0.001	1.016 (0.989, 1.044)	0.240	NA
TBIL (μmol/L)	0.477	< 0.001	1.042 (0.983, 1.103)	0.164	NA
DBiL (μmol/L)	0.514	< 0.001	0.982 (0.889, 1.085)	0.720	NA
IBiL (μmol/L)	0.417	< 0.001	0.879 (0.186, 4.161)	0.871	NA
CKMB (U/L)	0.323	< 0.001	1.075 (1.007, 1.148)	0.300	NA
CRP(mg/L)	0.410	< 0.001	0.989 (0.952, 1.028)	0.575	NA
PBNP (pg/mL)	0.382	< 0.001	1.001 (0.997, 1.005)	0.587	NA
HDL-C(mmol/L)	-0.235	< 0.001	0.532 (0.239, 1.184)	0.122	NA
MYO (ng/mL)	0.232	< 0.001	1.001 (0.998, 1.004)	0.571	NA
LP(mg/L)	-0.234	0.151	NA	NA	NA
Weight (kg)	0.050	0.530	NA	NA	NA
Diabetes	0.074	0.354	NA	NA	NA
Hypertension	-0.002	0.977	NA	NA	NA
ALT(U/L)	0.106	0.182	NA	NA	NA
CR (μmol/L)	0.085	0.286	NA	NA	NA
UA (μmol/L)	-0.098	0.217	NA	NA	NA
LDH (U/L)	-0.017	0.833	NA	NA	NA
TG(mmol/L)	-0.030	0.703	NA	NA	NA
Sex	0.113	0.156	NA	NA	NA
Height (cm)	0.021	0.788	NA	NA	NA
BMI (kg/m ²)	0.058	0.470	NA	NA	NA

Table 2. Clinical characteristics related to fibrosis. b coefficients are from multivariable logistic regression. Clinical variables found to be significantly related to fibrosis through spearman correlation analysis entered into logistic multivariate analysis. A/G albumin-globulin ratio, ALP alkaline phosphatase, ALT alanine aminotransferase, AST aspartate aminotransferase, CKMB creatine kinase-MB, CR creatinine, UR urea, UA uric acid, CRP C-reactive protein, DBiL direct bilirubin, GGT gamma-glutamyl transferase, HB hemoglobin, HDL-C high-density lipoprotein cholesterol, IBiL indirect bilirubin, LDH lactate dehydrogenase, LP lipoprotein, LDL-C low-density lipoprotein cholesterol, MYO myoglobin, PBNP Pro-B-type natriuretic peptide, RBC red blood cell, TBA total bile acid, TBIL total bilirubin, TC total cholesterol, TG triglyceride, WBC white blood cell.

diagnosis of advanced fibrosis and cirrhosis, respectively. The AUC results of FIB-4 were 0.801, 0.880 and 0.931, respectively. The AUC results of GPR were 0.750, 0.746 and 0.758, respectively (Table 3). We employed DeLong test statistics to compare the performance of different models. The Clinical-Radiomics_{arterial} model demonstrates robust predictive abilities in disease prognostication. Furthermore, the Radscore_{arterial}, APRI, GPR, and FIB-4 models exhibited varying degrees of predictive abilities (Table 4).

Feature reduction and establishment of radiomics model

1218 features were extracted from arterial phase, venous phase and delayed phase respectively, resulting in a total of 3654 features. Select stable features with high reproducibility through ICC for further analysis (684 arterial phase features, 645 venous phase features, 496 delayed phase features).

In the arterial phase, the LASSO and mRMR method identified a set of 10 features, including 3 first-order statistics, 6 texture features, and 1 wavelet-based transformations features. In the venous phase, 6 features were

Models	S01 vs. S234		S012 vs. S34		S0123 vs. S4	
	Training	Validation	Training	Validation	Training	Validation
APRI						
AUC (95% CI)	0.712 (0.671, 0.753)	0.757 (0.726, 0.787)	0.787 (0.762, 0.811)	0.796 (0.793, 0.799)	0.782 (0.758, 0.807)	0.821 (0.819, 0.823)
Specificity(%)	23.59	21.91	80.20	74.28	84.13	81.71
Sensitivity(%)	94.02	93.67	70.82	63.89	59.40	62.86
Accuracy (%)	68.24	57.79	76.21	70.17	75.16	76.21
GPR						
AUC (95% CI)	0.821 (0.796, 0.846)	0.750 (0.745, 0.754)	0.815 (0.790, 0.839)	0.746 (0.744, 0.747)	0.731 (0.680, 0.782)	0.758 (0.721, 0.795)
Specificity(%)	29.18	24.33	87.31	79.38	91.37	87.82
Sensitivity(%)	90.60	90.25	47.24	48.21	30.94	43.43
Accuracy (%)	68.46	57.29	69.96	67.04	68.90	74.88
FIB-4						
AUC (95% CI)	0.795 (0.758, 0.832)	0.801 (0.776, 0.826)	0.873 (0.853, 0.894)	0.880 (0.876, 0.884)	0.872 (0.851, 0.893)	0.931 (0.928, 0.935)
Specificity(%)	44.43	43.58	95.24	93.17	95.23	94.41
Sensitivity(%)	80.64	81.33	54.92	57.37	57.92	72.43
Accuracy (%)	68.27	62.42	77.63	79.00	81.29	88.00
Clinical						
AUC (95% CI)	0.791 (0.768, 0.815)	0.811 (0.808, 0.813)	0.911 (0.894, 0.927)	0.850 (0.849, 0.852)	0.884 (0.866, 0.903)	0.953 (0.951, 0.955)
Specificity(%)	59.87	50.33	91.72	89.03	93.5	95.88
Sensitivity(%)	89.82	84.42	84.54	71.68	75.56	67.14
Accuracy (%)	78.79	67.38	88.66	82.17	86.85	87.5
Radscore _{arterial}						
AUC (95% CI)	0.780 (0.747, 0.813)	0.839 (0.835, 0.844)	0.854 (0.833, 0.875)	0.816 (0.813, 0.818)	0.853 (0.829, 0.877)	0.870 (0.869, 0.871)
Specificity(%)	51.87	55.20	83.94	78.62	88.85	84.35
Sensitivity(%)	85.48	93.25	70.66	75.05	70.68	73.00
Accuracy (%)	73.24	74.38	78.30	77.21	82.14	81.04
Radscore _{venous}						
AUC (95% CI)	0.788 (0.763, 0.814)	0.816 (0.812, 0.820)	0.858 (0.872, 0.881)	0.884 (0.882, 0.886)	0.923 (0.904, 0.943)	1.000 (1.000- 1.000)
Specificity(%)	87.01	83.33	97.51	99.03	98.54	100
Sensitivity(%)	68.69	67.50	72.72	73.05	82.86	94.71
Accuracy (%)	75.71	75.42	86.69	88.75	92.66	98.46
Radscore _{delayed}						
AUC (95% CI)	0.782 (0.756, 0.808)	0.810 (0.806, 0.814)	0.859 (0.836, 0.881)	0.882 (0.880, 0.884)	0.920 (0.898, 0.941)	0.998 (0.997, 0.998)
Specificity(%)	86.60	83.67	95.91	96.97	98.02	99.59
Sensitivity(%)	68.88	67.75	73.40	72.53	83.36	93.29
Accuracy (%)	75.67	75.71	86.09	87.29	92.52	97.75
Clinical-radiomics _{arterial}						
AUC (95% CI)	0.833 (0.810, 0.855)	0.854 (0.851, 0.857)	0.923 (0.905, 0.940)	0.863 (0.861, 0.866)	0.909 (0.892, 0.927)	0.960 (0.958, 0.961)
Specificity(%)	66.44	67.92	95.01	87.93	95.34	93.94
Sensitivity(%)	88.87	85.33	85.91	74.63	82.67	70.29
Accuracy (%)	80.64	76.62	91.07	82.67	90.62	87.04
Clinical-radiomics _{venous}						
AUC (95% CI)	0.819 (0.798, 0.841)	0.836 (0.833, 0.838)	0.934 (0.918, 0.949)	0.862 (0.860, 0.864)	0.926 (0.909, 0.943)	0.997 (0.996, 0.997)
Specificity(%)	74.05	62.58	97.10	92.76	99.24	99.82
Sensitivity(%)	85.18	80.25	85.11	73.68	86.34	88.57
Accuracy (%)	81.31	71.42	91.89	85.21	94.42	96.54
Clinical-radiomics _{delay}						
AUC (95% CI)	0.821 (0.800, 0.842)	0.838 (0.835, 0.841)	0.932 (0.916, 0.947)	0.863 (0.862, 0.865)	0.924 (0.907, 0.941)	0.996 (0.996, 0.997)
Specificity(%)	74.98	63.42	95.88	92.00	98.08	99.82
Sensitivity(%)	84.78	80.33	86.92	73.68	86.44	88.14
Accuracy (%)	81.43	71.88	92.01	84.75	93.75	96.42

Table 3. Diagnostic performance of models for staging liver fibrosis. *APRI* aspartate transaminase to platelet ratio, *FIB-4* fibrosis 4 score, *GPR* gamma glutamyl transpeptidase to platelet ratio, *AUC* area under the curve.

Models	S01 vs. S234		S012 vs. S34		S0123 vs. S4	
	AUC (95% CI)	P value	AUC (95% CI)	P value	AUC (95% CI)	P value
Clinical-Radiomics _{arterial}	0.854 (0.831, 0.875)	NA	0.863 (0.849, 0.884)	NA	0.959 (0.948, 0.968)	NA
Radscore _{arterial}	0.839 (0.801, 0.865)	0.370	0.815 (0.800, 0.829)	<0.001	0.869 (0.861, 0.878)	<0.001
Clinical	0.810 (0.793, 0.824)	<0.05	0.850 (0.840, 0.863)	0.311	0.953 (0.943, 0.968)	0.741
APRI	0.728 (0.403, 0.789)	<0.001	0.794 (0.785, 0.817)	<0.001	0.821 (0.803, 0.833)	<0.001
GPR	0.740 (0.625, 0.769)	<0.001	0.745 (0.731, 0.755)	<0.001	0.769 (0.534, 0.800)	<0.05
FIB-4	0.789 (0.514, 0.820)	<0.001	0.880 (0.864, 0.885)	0.184	0.931 (0.903, 0.938)	<0.05

Table 4. DeLong test statistic Clinical-Radiomics_{arterial} vs. Radscore_{arterial}/Clinical/APRI/GPR/FIB-4. APRI aspartate transaminase to platelet ratio, FIB-4 fibrosis 4 score, GPR gamma glutamyl transpeptidase to platelet ratio, AUC area under the curve.

selected, consisting of 4 first-order statistics features and 2 texture features. In the delayed phase, 6 features were selected, comprising of 3 first-order statistics features and 3 texture features. These features were trained to staging fibrosis. The models was constructed using the SVC algorithm. All models were trained and validated using the parameters $C = 0.5$, $\gamma = \text{scale}$, $\text{kernel} = \text{rbf}$, $\text{probability} = \text{True}$, and with random state = 20.

As for the validation cohort, the radiomics models based on multi-phase CT images showed the performance with AUCs of 0.839 (95% CI 0.835–0.844), 0.816 (95% CI 0.813–0.818), 0.870 (95% CI 0.869–0.871) for the arterial phase; 0.816 (95% CI 0.812–0.820), 0.884 (95% CI 0.882–0.886), 1.000 (95% CI 1.000–1.000) for the venous phase; 0.810 (95% CI= 0.806–0.814), 0.882 (95% CI 0.880–0.884), 0.998 (95% CI 0.998–0.998) for the delay phase in the diagnosis of significant fibrosis (S01 vs. S234), advanced fibrosis (S012 vs. S34), and cirrhosis (S0123 vs. S4), respectively (Table 3).

The construction nomograms and decision curve analysis for Clinical-Radiomics

We developed the Clinical-Radiomics_{arterial} nomogram (Fig. 4) combines the Radscore_{arterial} with six clinical markers (PLT, ALP, A / G, UR, LDL-C, and TC). In the validation cohort, the AUCs for combination model of Clinical-Radiomics_{arterial} were 0.854 (95% CI 0.851–0.857), 0.863 (95% CI 0.861–0.866), 0.960 (95% CI 0.958–0.961) for differentiating significant fibrosis, advanced fibrosis, and cirrhosis, respectively; The AUCs of Clinical-Radiomics_{venous} were 0.836 (95% CI 0.833–0.838), 0.862 (95% CI 0.860–0.864), and 0.997 (95% CI 0.996–0.997); The AUCs of Clinical-Radiomics_{delay} were 0.838 (95% CI 0.835–0.841), 0.863 (95% CI 0.862–0.865), 0.996 (95% CI 0.996–0.997). The performance of the validation set was demonstrated in (Table 3).

The diagnostic performance of the Clinical-Radiomics_{arterial} model was outstanding in both the training and validation sets, warranting attention, with AUC values ranging from 0.833 to 0.923 and 0.854 to 0.960, with accuracy of 80.64–91.07% and 76.62–87.04% for staging fibrosis. The performance of the Clinical-Radiomics model was assessed using ROC analysis, as depicted in (Fig. 5). The performance of the Clinical-Radiomics_{arterial} model was evaluated using a matrix, as illustrated in (Fig. 6). Besides, we further evaluated the Clinical-Radiomics_{arterial} model in predicting liver fibrosis by DCA (Fig. 7). The DCA has shown that employing a Clinical-Radiomics nomogram to predict fibrosis status provides more benefit than treating all or none of the patients.

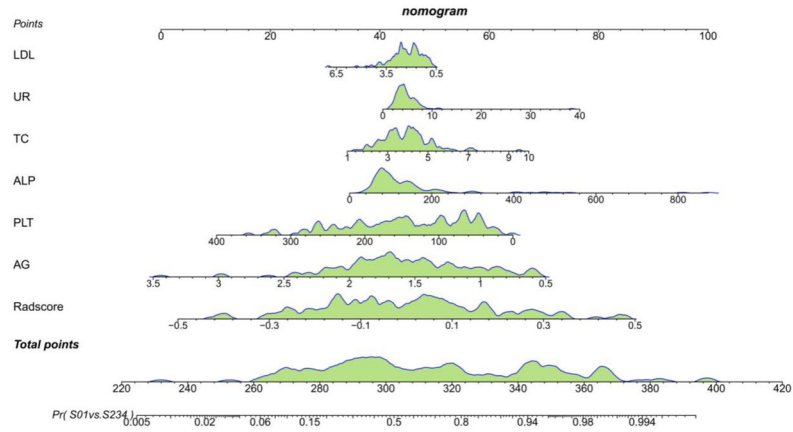
Discussion

The results of this study clearly demonstrate that the radiomics model is highly effective in distinguishing between various stages of liver fibrosis, exhibiting AUC values ranging from 0.810 to 1.000. The integration of clinical parameters with radiomics data further enhances diagnostic accuracy, as indicated by AUC values between 0.836 and 0.997 in the validation cohort, and achieves a commendable accuracy of 71.42 to 96.54% in staging hepatic fibrosis. Notably, these models have also been shown to significantly outperform traditional non-invasive biomarkers such as GPR, APRI, and FIB-4. The results indicate that the clinical-radiomics model manifests substantial potential as a sophisticated non-invasive diagnostic modality for the nuanced assessment and accurate staging of hepatic fibrosis, presaging enhanced patient management and prognostic outcomes.

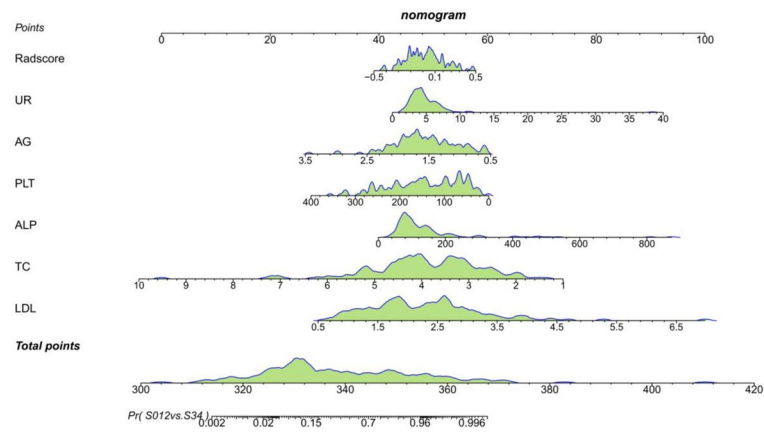
Previous study has suggested that elastography methods entails a higher cost compared to alternative non-invasive indicators²⁵, and CT-based radiomics has the potential to identify subtle alterations throughout the progressive stages of liver fibrosis²⁶. However, the study only included the extraction of radiomic features from 2D images at the portal vein level of liver, and did not compare the performance of arterial, venous, and delayed phase models based on multiphase CT images in radiomic models. In comparison, our study employed the trained 3D-UNet liver segmentation software for the automatic segmentation of the entire liver. Subsequently, we conducted a comparative analysis of multiphase CT images, encompassing the arterial phase, venous phase, and delayed phase. Hu et al. presented that venous phase CT images were chosen to develop and validate a CT-based radiomics nomogram for distinguishing between non-advanced and advanced liver fibrosis²⁷. Our research findings indicate that the model based on the Radscore_{arterial} shows a higher AUC in the significant fibrosis (S01vs. S234) group. Meanwhile, in the advanced fibrosis (S012vs.S34) and cirrhosis (S0123vs.S4) groups, the AUC of the the Radscore_{venous/delayed} model was higher.

Prior research have unveiled that FIB-4 excels in accurately identifying cirrhosis (F4) while displaying suboptimal performance in ruling out significant fibrosis ($\geq F2$), APRI exhibits solely moderate sensitivity and accuracy in appraising fibrosis connected to HBV²⁸. Previous studies also have demonstrated GPR

a S01 vs. S234



b S012 vs. S34



c S0123 vs. S4

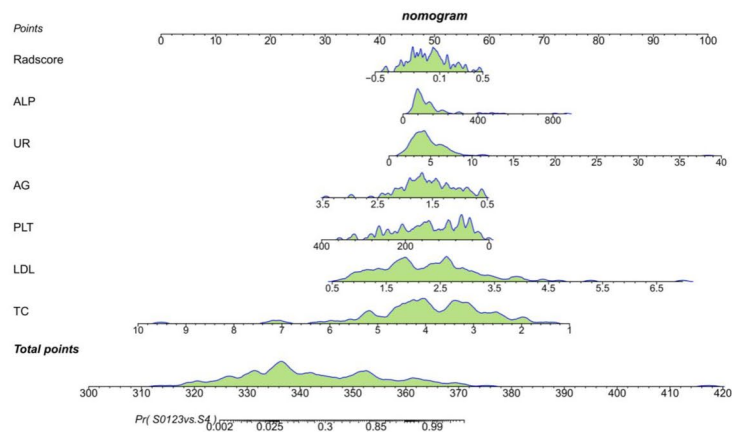


Fig.4. The nomograms of the Clinical-Radiomics_{arterial} model for evaluating fibrosis stage. Nomograms were constructed to evaluate significant fibrosis, advanced liver fibrosis and cirrhosis, respectively. Each variable specifies a point on the top axis by drawing a line upwards. The sum of these numbers is located on the “total points” axis, and a straight line is drawn down on the “probability” axis to calculate the likelihood of staging liver fibrosis.

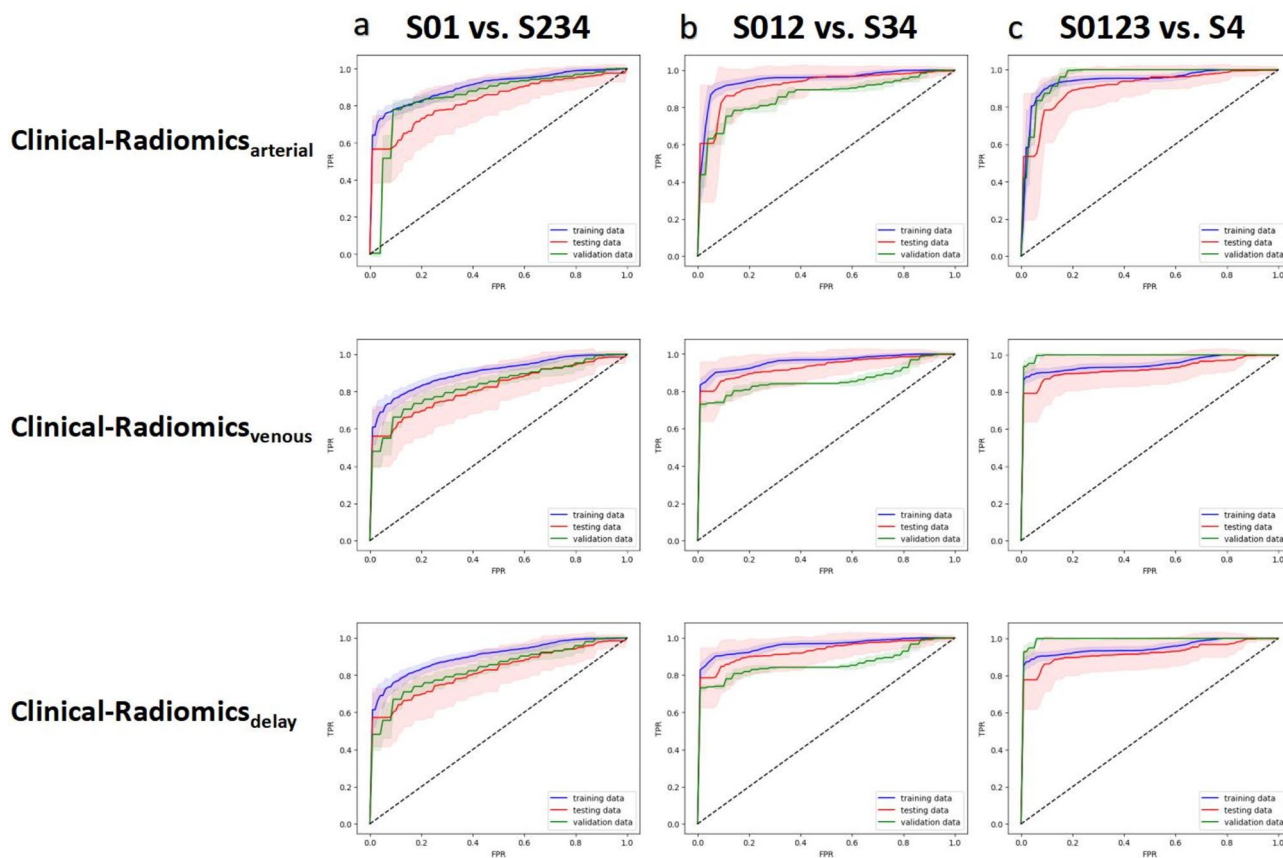


Fig.5. The ROC of the Clinical-Radiomics model for staging liver fibrosis in training and validation set.

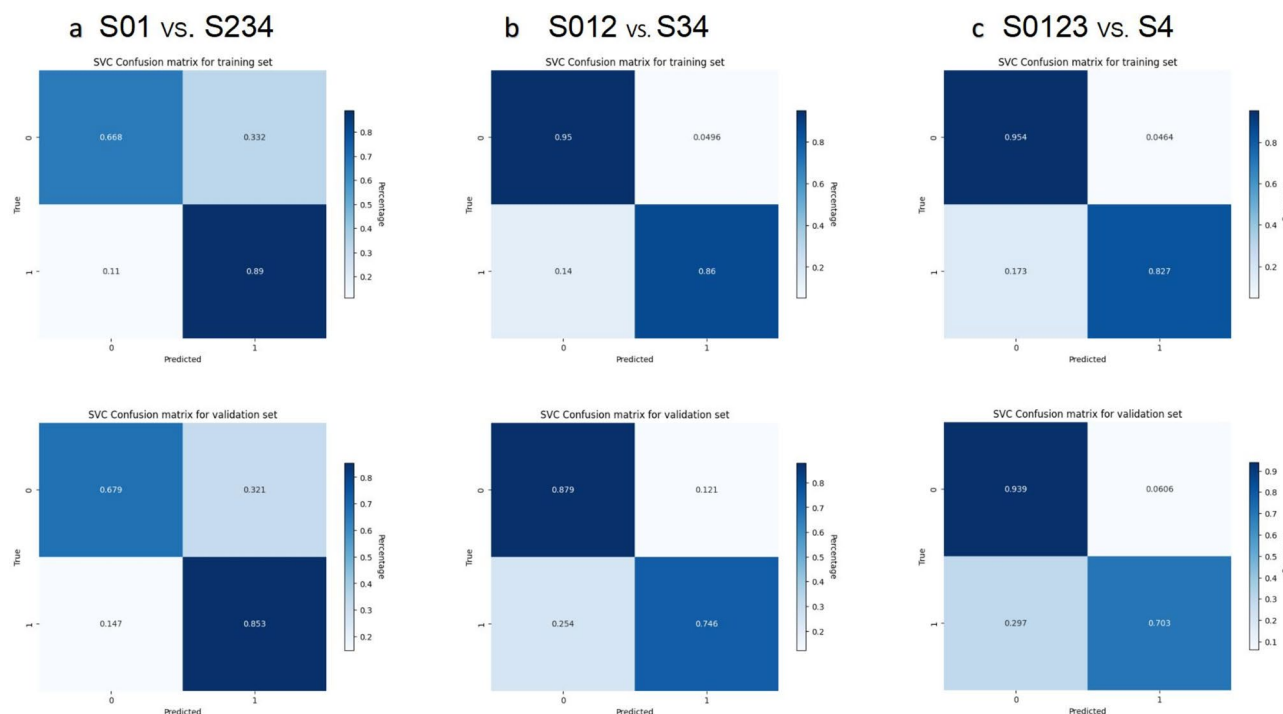
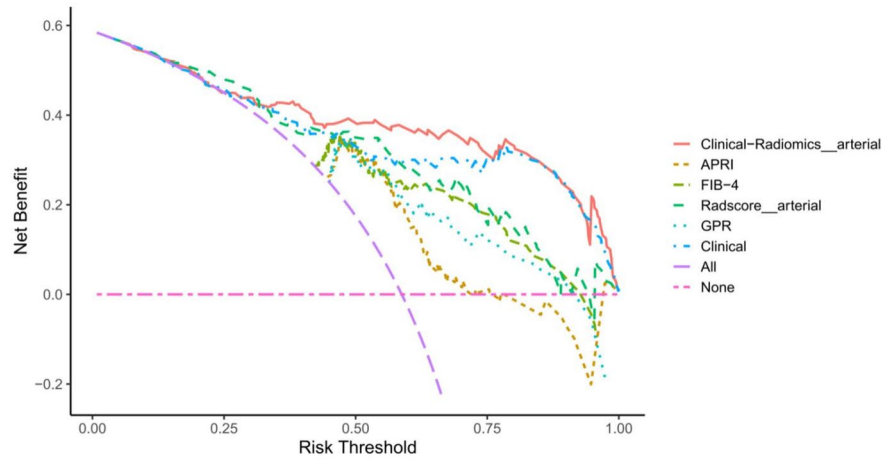
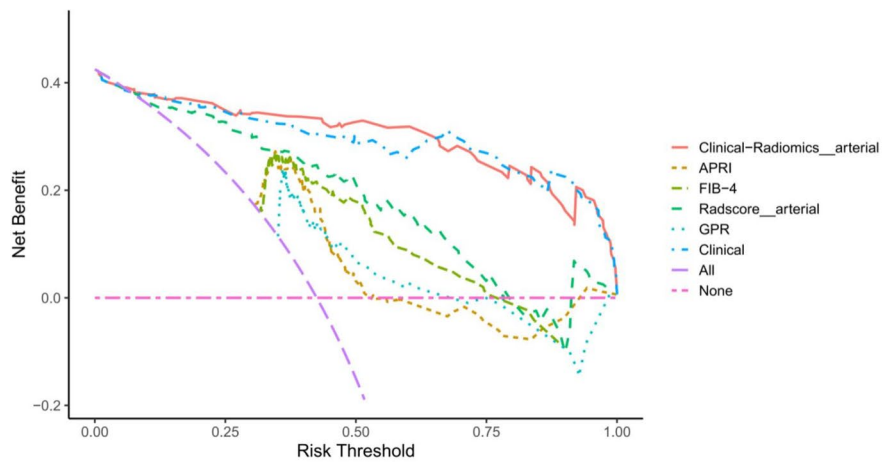


Fig.6. The confusion matrices of the Clinical-Radiomics_{arterial} model for staging liver fibrosis in the training and validation sets. Figures (a), (b), and (c) present confusion matrix plots showing the performance of the Clinical-Radiomics_{arterial} model on the training and validation sets.

a S01 vs. S234



b S012 vs. S34



c S0123 vs. S4

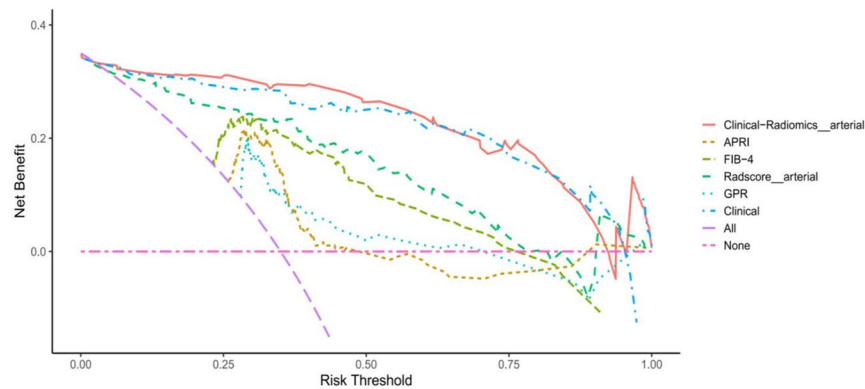


Fig.7. The decision curve analysis for models. The decision curve analysis delineates the net clinical benefit. None=no net benefit when no patients had fibrosis; All=net benefit when all patients experience the event.

is an inexpensive, simple, and easy-to-calculate model for anticipating the extent of liver fibrosis in patients with chronic hepatitis B²⁹. According to our results, the three specific clinical indicators were effective in determining the stage of liver fibrosis with the AUCs of 0.750–0.931 and accuracy of 57.29–88.00% in the validation set. However, the diagnostic efficacy is lower compared to our clinical-radiomics model.

Several constraints in this study should be noted. First, due to its retrospective nature, inherent selection biases are unavoidable. A future prospective, multicenter study addressing the same research question could

offer significant improvements. Second, the limited sample size of patients with F3 liver fibrosis in the current study poses a potential constraint, making machine learning models susceptible to the bias-variance tradeoff. Third, significant disparities in sample sizes for liver fibrosis across different etiologies hinder the realization of stratified research objectives. Finally, variations in CT scanners may impact the study's outcome.

Conclusion

We developed a combined prediction model utilizing multiphase CT-based radiomics features and clinical biomarker, and the combined model exhibited strong performance in predicting fibrosis stage with CLD patients. The clinical-radiomics nomogram has the potential to assist in clinical decision-making, offering potential benefits in the patients with CLD.

Data availability

The datasets generated during and/or analyzed during the current study are available from the corresponding author on reasonable request.

Received: 3 February 2024; Accepted: 22 August 2024

Published online: 30 August 2024

References

- Cheemera, S. & Balakrishnan, M. Global epidemiology of chronic liver disease. *Clin. Liver Dis. (Hoboken)* **17**(5), 365–370 (2021).
- Castera, L. Invasive and non-invasive methods for the assessment of fibrosis and disease progression in chronic liver disease. *Best Pract. Res. Clin. Gastroenterol.* **25**(2), 291–303 (2011).
- Bravo, A. A., Sheth, S. G. & Chopra, S. Liver biopsy. *N. Engl. J. Med.* **344**(7), 495–500 (2001).
- Lomba, R. & Adams, L. A. Advances in non-invasive assessment of hepatic fibrosis. *Gut* **69**(7), 1343–1352 (2020).
- Grigorescu, M. Noninvasive biochemical markers of liver fibrosis. *J. Gastrointest. Liver Dis.* **15**(2), 149–159 (2006).
- Lubner, M. G., Malecki, K., Kloke, J., Ganeshan, B. & Pickhardt, P. J. Texture analysis of the liver at MDCT for assessing hepatic fibrosis. *Abdom. Radiol. (NY)*. **42**(8), 2069–2078 (2017).
- Herrmann, E. *et al.* Assessment of biopsy-proven liver fibrosis by two-dimensional shear wave elastography: An individual patient data-based meta-analysis. *Hepatology*. **67**(1), 260–272 (2018).
- Singh, S. *et al.* Diagnostic performance of magnetic resonance elastography in staging liver fibrosis: A systematic review and meta-analysis of individual participant data. *Clin. Gastroenterol. Hepatol.* **13**(3), 440–451.e6 (2015).
- Xiao, G. *et al.* Comparison of laboratory tests, ultrasound, or magnetic resonance elastography to detect fibrosis in patients with nonalcoholic fatty liver disease: A meta-analysis. *Hepatology* **66**(5), 1486–1501 (2017).
- Marrero, J. A. *et al.* Diagnosis, staging, and management of hepatocellular carcinoma: 2018 practice guidance by the American association for the study of liver diseases. *Hepatology* **68**(2), 723–750 (2018).
- Wang, J. *et al.* Radiomics analysis of contrast-enhanced CT for staging liver fibrosis: An update for image biomarker. *Hepatol. Int.* **16**(3), 627–639 (2022).
- Gillies, R. J., Kinahan, P. E. & Hricak, H. Radiomics: Images are more than pictures. *Data. Radiol.* **278**(2), 563–577 (2016).
- Wei, J. *et al.* Radiomics in liver diseases: Current progress and future opportunities. *Liver Int.* **40**(9), 2050–2063 (2020).
- Mokrane, F. Z. *et al.* Radiomics machine-learning signature for diagnosis of hepatocellular carcinoma in cirrhotic patients with indeterminate liver nodules. *Eur. Radiol.* **30**(1), 558–570 (2020).
- Ji, G. W. *et al.* Machine-learning analysis of contrast-enhanced CT radiomics predicts recurrence of hepatocellular carcinoma after resection: A multi-institutional study. *EBioMedicine* <https://doi.org/10.1016/j.ebiom.2019.10.057> (2019).
- Liu, F. *et al.* Development and validation of a radiomics signature for clinically significant portal hypertension in cirrhosis (CHESS1701): A prospective multicenter study. *EBioMedicine* <https://doi.org/10.1016/j.ebiom.2018.09.023> (2018).
- Park, H. J. *et al.* Radiomics analysis of gadoxetic acid-enhanced MRI for staging liver fibrosis. *Radiology*. **290**(2), 380–387 (2019).
- Zhou, Z. *et al.* Liver fibrosis assessment using radiomics of ultrasound homodyned-k imaging based on the artificial neural network estimator. *Ultrason. Imaging*. **44**(5–6), 229–241 (2022).
- Zhang, D. *et al.* Radiomics nomograms based on R2* mapping and clinical biomarkers for staging of liver fibrosis in patients with chronic hepatitis B: A single-center retrospective study. *Eur. Radiol.* **33**(3), 1653–1667 (2023).
- Scheuer, P. J. Classification of chronic viral hepatitis: A need for reassessment. *J. Hepatol.* **13**(3), 372–374 (1991).
- O'Brien, R. M. A caution regarding rules of thumb for variance inflation factors. *Quality Quantity* <https://doi.org/10.1007/s11135-006-9018-6> (2007).
- Wai, C. T. *et al.* A simple noninvasive index can predict both significant fibrosis and cirrhosis in patients with chronic hepatitis C. *HEPATOLOGY* **38**(2), 518–526 (2010).
- Vallet-Pichard, A. *et al.* FIB-4: an inexpensive and accurate marker of fibrosis in HCV infection comparison with liver biopsy and fibrotest. *Hepatology* <https://doi.org/10.1002/hep.21669> (2007).
- Lemoine, M. *et al.* The gamma-glutamyl transpeptidase to platelet ratio (GPR) predicts significant liver fibrosis and cirrhosis in patients with chronic HBV infection in West Africa. *Gut* **65**(8), 1369–1376 (2016).
- EASL-ALEH Clinical Practice Guidelines. Non-invasive tests for evaluation of liver disease severity and prognosis. *J. Hepatol.* **63**(1), 237–264 (2015).
- Wang, J. C. *et al.* A radiomics-based model on non-contrast CT for predicting cirrhosis: Make the most of image data. *Biomark Res.* <https://doi.org/10.1186/s40364-020-00219-y> (2020).
- Hu, P. *et al.* A combination model of radiomics features and clinical biomarkers as a nomogram to differentiate nonadvanced from advanced liver fibrosis: A retrospective study. *Acad. Radiol.* <https://doi.org/10.1016/j.acra.2020.08.029> (2021).
- Zeng, D. W., Dong, J., Liu, Y. R., Jiang, J. J. & Zhu, Y. Y. Noninvasive models for assessment of liver fibrosis in patients with chronic hepatitis B virus infection. *World J. Gastroenterol.* **22**(29), 6663–6672 (2016).
- Purkayastha, S., Jha, A. K., Kumar, R., Dayal, V. M. & Jha, S. K. Serum gamma-glutamyl transpeptidase-to-platelet ratio as a noninvasive marker of liver fibrosis in chronic hepatitis B. *Cureus*. **15**(1), e33744 (2023).

Acknowledgements

The authors gratefully thank all the participants at Guizhou Medical University; we are also thankful to Study-ForBetter Team who contributed their best research spirits to this work.

Author contributions

Writing—original draft, Methodology, Data curation, Formal analysis, Validation: [Maowen Tang], Writing—original draft, Methodology, Data curation, Visualization, Software. [Yuhui Wu], Writing—review & editing, Methodology, Data curation, Investigation. [Na Hu], Data curation, Writing—review & editing, Formal analysis:[Chong Lin], Data curation, Writing—review & editing:[Jian He], Writing—review & editing, Methodology:[Xing Xia, Meihua Yang], Writing—review & editing, Supervision, Formal analysis, Conceptualization, Funding acquisition:[Pingui Lei, Peng Luo]. All authors reviewed the manuscript.

Funding

Funding for the Excellent Reserve Talents in the Discipline of Affiliated Hospital of Guizhou Medical University,gyfyxkyc-2023-13,Guizhou Provincial Science and Technology Projects,Qiankehejichu-ZK[2023]353,Cultivation Project of National Natural Science Foundation of China by The Affiliated of Guizhou Medical University,gyfyfnsfc[2023] -03,Guizhou Province High-level Innovative Talent Program,gzwijsr 2023-019.

Competing interests

The authors declare no competing interests.

Additional information

Correspondence and requests for materials should be addressed to P.L. or P.L.

Reprints and permissions information is available at www.nature.com/reprints.

Publisher's note Springer Nature remains neutral with regard to jurisdictional claims in published maps and institutional affiliations.

Open Access This article is licensed under a Creative Commons Attribution-NonCommercial-NoDerivatives 4.0 International License, which permits any non-commercial use, sharing, distribution and reproduction in any medium or format, as long as you give appropriate credit to the original author(s) and the source, provide a link to the Creative Commons licence, and indicate if you modified the licensed material. You do not have permission under this licence to share adapted material derived from this article or parts of it. The images or other third party material in this article are included in the article's Creative Commons licence, unless indicated otherwise in a credit line to the material. If material is not included in the article's Creative Commons licence and your intended use is not permitted by statutory regulation or exceeds the permitted use, you will need to obtain permission directly from the copyright holder. To view a copy of this licence, visit <http://creativecommons.org/licenses/by-nc-nd/4.0/>.

© The Author(s) 2024